13

New Trends in Materials Nondestructive Characterization Using Surface Acoustic Wave Methodologies

T. E. Matikas and D. G. Aggelis
Materials Science & Engineering Department,
University of Ioannina, Ioannina,
Greece

1. Introduction

The surface of the materials is usually the most sensitive part due to exposure to environmental influence, as well as higher bending and torsional loads than the interior. Therefore, degradation is bound to initiate from the surface in most engineering components. Surface wave propagation in heterogeneous media is a topic concentrating many efforts in the engineering community. The main aim is quality characterization via nondestructive evaluation (NDE) methodologies by correlation of propagation characteristics with material properties. In the present chapter surface waves are examined in structural materials of outmost significance such as aerospace composites and concrete.

Concrete structures are exposed to deterioration factors like weathering, corrosive agents, thermal expansion and contraction or even freezing and thawing. Additionally, they support operation loads, own weight and possibly dynamic overloading by earthquakes. Most of the above factors affect primarily the surface of structures, which is directly exposed to the atmospheric conditions and sustain maximum flexural loads. Deterioration therefore, is bound to start from the surface in most cases. This deterioration may be manifested in the form of large surface breaking cracks and/or distributed micro-cracking in the surface layer of the material. Inspection techniques based on the propagation of elastic waves have been long used for the estimation of the quality and general condition of the material [1,2] either in through the thickness or in surface mode. Surface wave propagation is complicated in that different kinds of waves co-exist. Normally the Rayleigh waves occupy most of the energy, while the longitudinal are the fastest [3,4]. Therefore, measuring the transit time of the first detectable disturbance of the waveform, leads to the calculation of the longitudinal wave velocity. This is referred to as pulse velocity [1-3] and it is widely used for rough correlations with quality. Other forms of wave speed are the phase velocity, which is calculated either by some characteristic point in the middle of a tone-burst of a specific frequency [5,6], or by spectral analysis of a broadband pulse [7]. Additionally, group velocity is calculated by the maximum peak, the maximum of the wave envelope, or cross-correlation between the "input" and "output" waveforms [8,9]. In homogeneous media all

these forms of velocity are expected to share the same value. However, for inhomogeneous media it has been shown that these velocities are not necessarily close [5,10].

From the above forms of velocity, the most common measurement in ultrasonics is the "pulse velocity". Considering that the material is homogeneous, pulse velocity is directly related to the elasticity modulus [11] and correlated to the strength of concrete through empirical relations [1,11-13]. Since it is measured by the first detectable disturbance of the waveform this measurement depends on the strength of the signal with respect to the noise, which could have environmental and equipment-induced components. In case the initial arrivals of the wave are weaker than or similar to the noise level, pulse velocity is underestimated. This could certainly be the case in actual structures, where propagation distances through damaged materials are usually long. Rayleigh waves are also excited in a concrete surface; they propagate within a penetration depth of approximately one wave length and carry more of the excitation energy [3,14]. Their velocity is also related to elasticity and Poisson's ratio. Measurement of Rayleigh velocity is usually conducted by a reference peak point, so it is not directly influenced by noise level [11]. However, for cases of severe damage or long propagation, the strong reference cycle used for the measurement is severely distorted making the selection of reference points troublesome [8,15], as will be seen later. Frequency domain techniques like phase difference calculation between signals recorded at specific distances may provide solution for velocity measurement revealing also the dependence of velocity on frequency [7,16].

In addition to wave velocity, attenuation has also been widely used for characterization of microstructural changes or damage existence [17,18]. It represents the reduction of the wave amplitude per unit of propagation length. Attenuation is more sensitive to damage or void content as has been revealed in several studies [5,8,18-20] and has been correlated to the size of the aggregates, as well as air void size and content in hardened and fresh cementitious materials [5,18]. The sensitivity of attenuation to the microstructure is such, that the content of "heterogeneity" is not the only dominating factor; the typical size and shape of the inclusions play an equivalently important role and therefore, Rayleigh wave attenuation has been related to parameters like aggregate size, and damage content [8,21-23]. This sensitivity to the microstructure may complicate assessment but on the other hand offers possibilities for more accurate characterization.

Accurate characterization would require determination of several damage parameters like the number (or equivalent damage content) of the cracks, their typical size, as well as their orientation. Though this is a nearly impossible task, especially in-situ, advanced features sensitive to the above damage parameters should be continuously sought for in order to improve the maintenance services in structures. The valuable but rough characterization based on pulse velocity can be improved by the addition of features from frequency domain as will be explained below.

Elastic waves are applied on the surface of mortar specimens with inhomogeneity. In order to simulate damage, small flakey inclusions were added in different contents and sizes, and parameters of the surface waves are calculated. The effect of "damage" content as well as the size of the inclusions on wave parameters is discussed showing that the typical size of inhomogeneity is equally important to the content. In similar studies, sphere is a first approximation for the damage shape, which produces quite reliable results [24]. However,

for the case of actual cracks, which were simulated by thin, flakey, light inclusions, the random orientation and general shape complicates the anticipated results and increases experimental scatter. This study aims to supply more experimental data in the area of surface waves in media with random and randomly oriented inhomogenity, which has not been studied as widely as stratified media [11,25] and media with surface breaking cracks [26-29]. The results presented herein are realistic due to the shape of the light inclusions, while size and population of inclusions leave their fingerprint on the phase velocity and attenuation curves since large population of small inclusions impose stronger attenuation that small population of larger size. Additionally the application of other features from frequency domain, like the coherence function, is discussed as to their contribution in damage characterization.

Concerning aerospace materials, innovative NDE methods based on linear and nonlinear acoustics are of outmost importance for developing damage tolerance approaches by monitoring the accumulation of damage under cyclic loading.

High strength titanium alloys, as well as fiber reinforced metal matrix composite materials, are being considered for a number of applications because of their improved mechanical properties in high temperature applications. In applications where cyclic loading is expected and where life management is required, consideration must be given to the behavior of the material in the vicinity of stress risers such as notches and holes. It is in these regions that damage initiation and accumulations are expected. In the case of metal matrix composites for aircraft structural and engine components, several damage modes near stress risers have been identified [30]. One important damage mode under cyclic loading is the nucleation and growth of matrix cracks perpendicular to the fiber direction. In some composite systems, the matrix crack growth occurs without the corresponding failure of the fibers. This process results in the development of relatively large matrix cracks that are either fully or partially bridged by unbroken fibers. The presence of bridging fibers can significantly influence the fatigue crack growth behavior of the composite. To develop a life prediction methodology applicable to these composite systems, an understanding must be developed of both the matrix cracking behavior as well as the influence of the unbroken fibers on the crack driving force and the effect of interfacial degradation and damage on the eventual failure of the composite.

Paramount to understanding the influence of unbroken fibers is to identify the mechanisms which transfer the load from the matrix to the fiber. The mechanics of matrix cracking and fiber bridging in brittle matrix composites has been addressed [31,32]. The analysis is based on the shear lag model to describe the transfer of load from the fiber to the matrix. In the shear lag model, the transfer of load occurs through the frictional shear force (τ) between the fiber and the matrix. The analyses indicate that size of the region on the fiber over which t acts can have a significant effect on the influence of unbroken fibers on crack growth rate behavior. However, although some indirect ultrasonic experimental techniques have been developed to determine the extent of influence of τ [33-35], no direct nondestructive experimental techniques currently exist. Another important interfacial phenomenon is the degradation, fracture and/or failure of the interface resulting from crack initiation and growth [36,37].

This chapter has an objective to discuss the utility and versatility of surface waves application in cementitious materials as well as two state-of-the-art surface acoustic wave techniques, ultrasonic microscopy and nonlinear acoustics, for material behavior research of aerospace materials.

Ultrasonic microscopy utilizes high focused ultrasonic transducers to induce surface acoustic waves in the material which can be successfully used for local elastic property measurement, crack-size determination, as well as for interfacial damage evaluation in high temperature materials, such as metal matrix composites [38]. Nonlinear acoustics enables real-time monitoring of material degradation in aerospace structures [39]. When a sinusoidal ultrasonic wave of a given frequency and of sufficient amplitude is introduced into a non-harmonic solid the fundamental wave distorts as it propagates, and therefore the second and higher harmonics of the fundamental frequency are generated. Measurements of the amplitude of these harmonics provide information on the coefficient of second and higher order terms of the stress-strain relation for a nonlinear solid. As it is shown here, the material bulk nonlinear parameter for metallic alloy samples at different fatigue levels exhibits large changes compared to linear ultrasonic parameters, such as velocity and attenuation [40].

2. Damage characterization in concrete using surface waves

In order to characterize damage, several parameters are required. These include the quantification of: damage content, typical size of cracking or even distribution of sizes and possibly orientation preference. This task is nearly impossible in real structures or even in laboratory due to several variables that need to be determined. However, dealing with some of the aspects of characterization is extremely important bearing in mind that so far, the assessment of concrete condition is based on the rough and empirical correlations between pulse velocity and strength. In the next part, the simulated damage content and typical size of cracks in concrete are examined in terms of their influence on different parameters of the propagating wave studied complementary to the conventional pulse velocity.

2.1 Experimental process

Concerning the part of the study relevant to cementitious materials, the experimental specimens were made of cement mortar with water to cement ratio of 0.5 and sand to cement 2 by mass. The maximum sand grain size was 3 mm. Two minutes after the ingredients were mixed in a concrete mixer, vinyl inclusions were added and the mixing continued for two additional minutes. Then the mixture was cast in square metal forms of 150 mm side. The specimens were demolded one day later and cured in water for 28 days [41]. The vinyl inclusions were added in different volume contents (specifically 1%, 5% and 10%), while a mortar specimen was also cast without any inclusions. Vinyl inclusions were cut in small square coupons from sheets with thickness of 0.2 mm and 0.5 mm. The exact sizes of the vinyl coupons were 15x15x0.5 mm, 15x15x0.2, 30x30x0.5 and 30x30x0.2 mm. One specimen was cast for each inclusion size and content.

After fracturing one preliminary specimen, it was revealed that the dispersion of the fillers can be considered random, as would possibly be the case for actual cracks. Although the total volume content of the fillers was strictly measured to the specified value (i.e. 1%, 5% and 10%) in order to exclude local variations twenty measurements were taken on the surface and the results were averaged.

For the ultrasonic measurements, three broadband piezoelectric transducers, Fujiceramics 1045S, were placed on the specimens' surface with a distance of 20 mm, see Fig. 1. A

pencil lead break was excited (HB 0.5) producing frequencies in the bandwidth of 0–300 kHz, in front of the first receiver. The signals received by the three sensors were preamplified by 40 dB and digitized with a sampling rate of 10 MHz in a Mistras system of Physical Acoustics Corporation. Silicone grease was used as couplant between the sensors and the specimen.

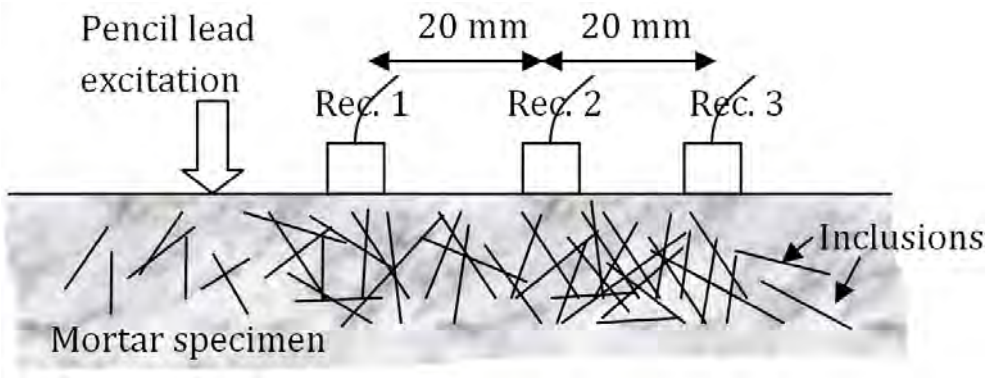

Fig. 1. The experimental setup.

2.2 Shape distortion and pulse velocity

Figure 2a shows typical waveforms as captured by the first and last receivers on a plain mortar specimen. In both receivers the strong Rayleigh cycle is observed, preceded by the weaker longitudinal mode. Measuring the delay between the strong negative peaks (Fig. 2a), the Rayleigh velocity is calculated at 2116 m/s. When simulated damage is included in a content of 1%, the Rayleigh cycle is slightly distorted (Fig. 2b). The Rayleigh velocity in this case is measured at the value of 2062 m/s. It is mentioned that the pulse velocity, dictated by the first detectable disturbance of the waveforms, is essentially similar for both cases measured at around 4140 m/s, meaning that Rayleigh waves are more sensitive to the slight amount of simulated damage than longitudinal. When the content of damage is 10% (see Fig. 2c) the Rayleigh cycle is severely distorted and a reference point cannot be easily selected for the measurement. In case the minimum point of the 2nd cycle is chosen (marked by an arrow), the Rayleigh velocity is calculated at 1770 m/s, being reduced by 17% relatively to the sound material, while pulse velocity is measured at 3773 m/s, with a corresponding decrease of 8.5%.

Figure 3 depicts the average longitudinal wave velocity for different types of inclusions and constant content of 5% normalized to the velocity of plain mortar. As observed, the different size has considerable effect on the velocity since the inclusions of 15x15x0.5 mm size reduce the velocity to approximately 96.5% of plain mortar while inclusions of 30x30x0.2 mm reduce the velocity even to 83%. This shows that the material cannot be treated as homogeneous considering only the volume fraction of inclusions (or cracks in an actual situation), since their shape and size is also important. The velocities presented come from the average of 20 individual measurements.

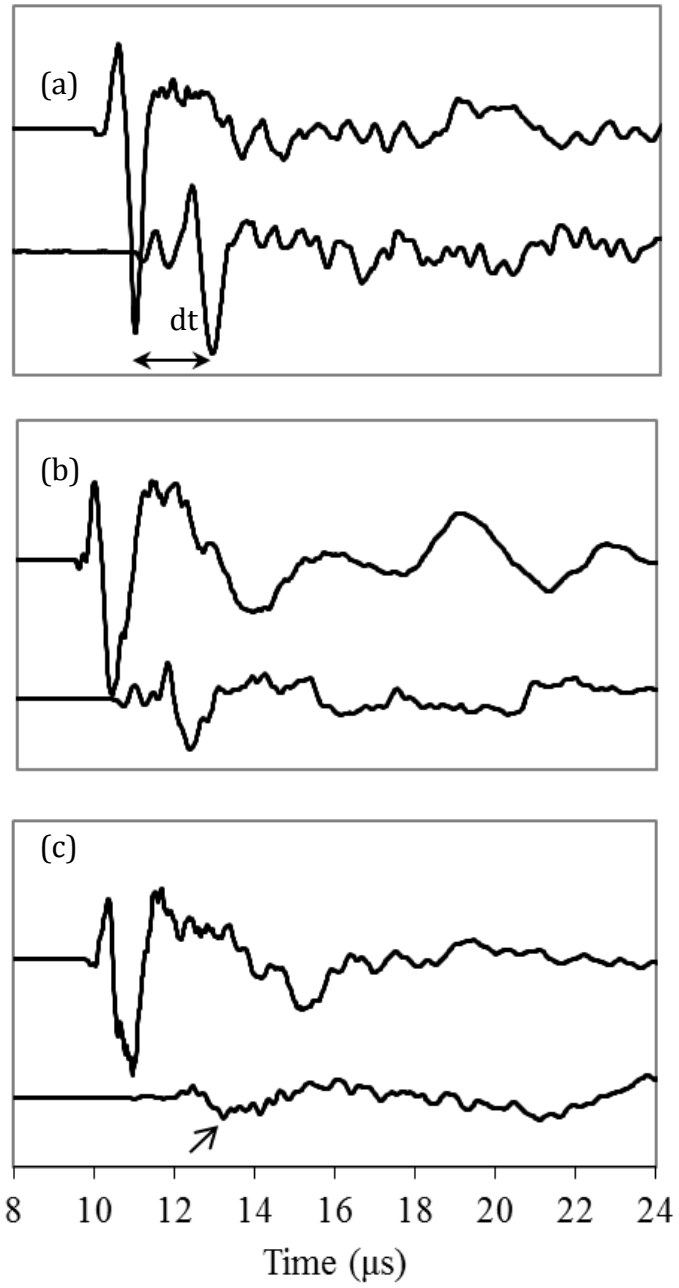

Fig. 2. Sample waveforms of 1st and 3rd receiver for mortar with inclusions contents 0% (a), 1% (b) and 10% (c) and inclusion size 30x30x0.5 mm.

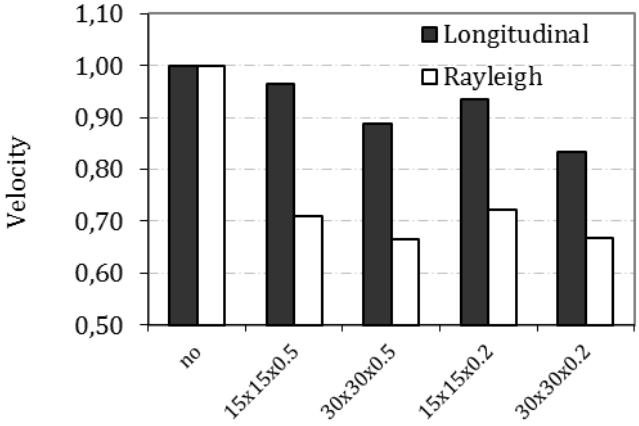

Fig. 3. Wave velocities for different inclusion sizes and constant content (5%).

As to the Rayleigh wave propagation, if a reference point can be identified, e.g. the strong negative peaks in Fig. 2(a), the Rayleigh velocity can be calculated easily. However, in case of strong distortion, case of Fig. 2(c) selection of a single point would not be safe. Therefore, an approach with cross-correlation was followed. The time lag resulting after cross correlation between the signals, over the separation distance between the first and third transducer (40 mm), gives a measure of the velocity with which the energy propagates [8]. For this task the first 100 μs of the waveforms were used where the Rayleigh contribution is certain to exist.

The results are shown again in Fig. 3 normalized to the plain mortar Rayleigh velocity of 2116m/s. The Rayleigh velocity follows similar diminishing trend with the longitudinal, being however more strongly reduced, to even 66% of the plain mortar, for the case of 30x30x0.2 inclusions. This again shows the importance of the scatterer size. Additionally, the differential influence of inclusion shape on longitudinal and Rayleigh wave velocities should be highlighted. This is another indication of the inhomogeneous nature of the material. The addition of lower elasticity inclusions reduces the "effective" modulus of elasticity of mortar. In case the material could be regarded as homogeneous, the influence on longitudinal and Rayleigh velocities should be the same, since they are both firmly connected to the elastic properties. However, for the material at hand, the Rayleigh is obstructed much more intensively, especially by the thin inclusions, showing that a traditional homogenized approach used for concrete is not adequate for cementitious material with inclusions. This should also be related to the propagation mechanism of Rayleigh waves, which includes displacement components in two directions (parallel and vertical to the direction of propagation) being therefore more sensitive to inhomogeneity.

2.3 Phase velocity

The above mentioned approach yields a measure of the velocity of the whole pulse. In a heterogeneous medium like the one studied herein, the velocity is expected to be strongly dependent on the frequency. Therefore, it is significant to calculate the dispersion curve (phase velocity vs. frequency). In the case of Rayleigh waves this is not trivial since there are

always contributions from longitudinal and shear waves that are faster. Therefore, the Rayleigh cannot be isolated. However, since they generally carry more energy than the other types, concentrating on a time window where the Rayleigh are expected, can yield information about this wave with little influence from other types. In this case a window of 30 μs located around the major Rayleigh arrivals was isolated and the rest of the waveform was zero-padded as presented in similar cases [42]. Using Fast Fourier Transform, the phase of the waveform is calculated and unwrapped. Therefore, the difference of phase between waveforms collected at different distances from the excitation (i.e. the first and third receiver) leads to the calculation of phase velocity vs. frequency curve [7]. The results are depicted in Fig. 4 for materials with different inclusion type and volume content 5%. Each curve is the average of 20 individual curves in order to diminish variation effects.

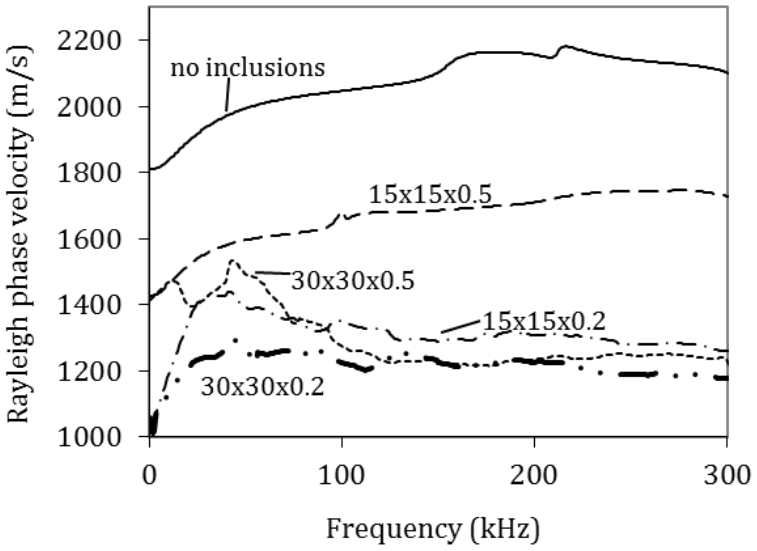

Fig. 4. Phase velocity vs. frequency curves for different size of inclusions and content 5% by vol.

It is seen that even plain mortar exhibits dispersive behavior with velocity increasing throughout the first 200 kHz. The dispersion curve for inclusions with dimensions 15x15x0.5 is translated to lower levels by about 400 m/s. However, other inclusion sizes seem to have much stronger influence, with the large and thin inclusions (30x30x0.2) lowering the curve by more than 800 m/s in average. Additionally, all the curves exhibit strong velocity increase for the band up to 50 kHz or 60 kHz. For higher frequencies each curve seems to converge. This is a behavior generally observed in composite systems. For low frequencies, the velocity may exhibit strong variations or resonance peaks but, as the frequency increases, the variations seem to diminish [43-44] as is the case for this study.

It is mentioned that the level of the dispersion curve is not necessarily close to the value of Rayleigh velocity measured by cross-correlation. For plain mortar, the Rayleigh phase velocity curve seen in Fig. 4, averages at 2073 m/s being close to the Rayleigh velocity of

2116 m/s measured by cross-correlation. However, as the inhomogeneity increases, considerable discrepancies arise. Indicatively, for the inclusions of 30x30x0.2 mm the phase velocity curve of Fig. 4 averages at 1217 m/s, while the cross-correlation leads to a velocity of 1426 m/s, see Fig. 3. This discrepancy has been observed in other cases of cementitious materials and increases with the level of inhomogeneity, i.e. from cement paste to mortar with sand grains or concrete with large aggregates [5], as well as other strongly scattering systems [10]. This trend is reasonable because in heterogeneous, dispersive materials the pulse shape changes during propagation and the expressions of velocity may well differ as they depend on the reference points selected for the calculation.

2.4 Spectral distortion

Apart from the velocity decrease, which is approximately of the order of 35% for Rayleigh waves, the signal suffers strong distortion which is evident from the shape of the time domain waveform. The distortion of the spectral content can be evaluated by the coherence function [45]. The frequency dependent coherence $\gamma_{xy}(f)$ between two time domain waveforms x(t) and y(t) is a measure of the similarity of their spectral content and can be described as the corresponding of cross-correlation in the frequency domain. It is given by:

$$\gamma_{xy}^2(f) = \frac{\left|G_{xy}(f)\right|^2}{G_{xx}(f)G_{yy}(f)},\ 0 \le \gamma_{xy}^2(f) \le 1 \tag{1}$$

where $G_{xy}(f)$ is the cross-spectral density function between time domain waveforms x(t) and y(t), while G_{xx} and G_{yy} are the auto-spectral density functions of x(t) and y(t).

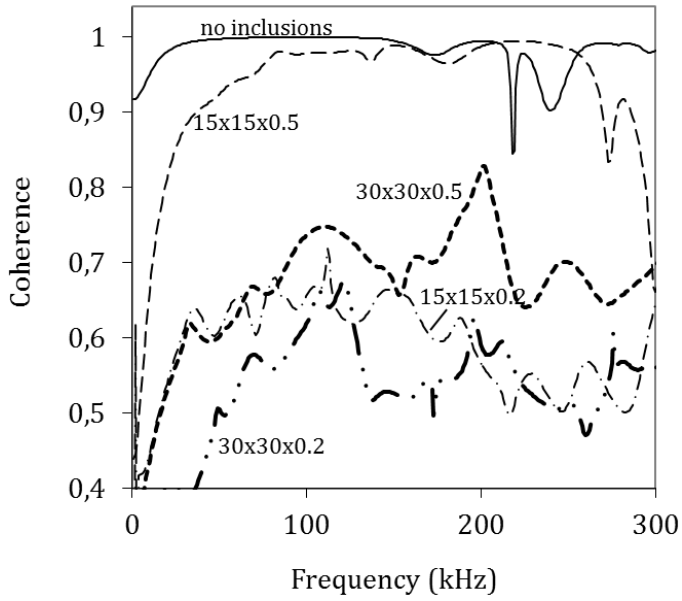

Fig. 5. Coherence function for different size of inclusions and content 5% by vol.

Figure 5 shows the coherence between signals collected at separation distance of 40 mm in mortar with different typical sizes of inhomogeneity. For no inclusions, the coherence is almost maximum (value close to 1), showing little distortion. Addition of inclusions in the content of 5% certainly diminishes the level of coherence but the result strongly depends on the size of the heterogeneity as well. Specifically for the size of 15x15x0.5 mm the average coherence is 0.92, while for 30x30x0.5 mm is 0.66. The lowest coherence is exhibited between signals recorded in specimens with 30x30x0.2 mm inclusions with an average value of 0.54. This shows the importance of the dominant size of inhomogeneity in spectral similarity and makes coherence a descriptor with strong characterizing power over the typical size of damage. It has also been used for characterization of concrete composition through ultrasonic signals and classification of acoustic emission signals [13,46].

2.5 Attenuation curves

The comparison of the peak amplitude of waveforms captured at different positions is a measure of attenuation. If the time domain signals are transformed into the frequency domain by fast Fourier transform (FFT) their response leads to the frequency dependent attenuation coefficient through the next equation:

$$a(f) = -\frac{20}{x}\log\left(\frac{A(f)}{B(f)}\right) \tag{2}$$

where a(f) is the attenuation coefficient with respect to frequency, A(f) and B(f) are the FFTs of the responses of the two sensors and x is the distance between the sensors (in this case 40 mm).

a(f) reveals the attenuative characteristics for specific frequency bands improving the characterization capacity, especially in controlled laboratory conditions, since the typical size of inhomogeneity affects specific wavelengths. Attenuation curves were calculated according to Eq. 2 for different inclusion contents and are seen in Fig. 6 for material with inclusion size of 30x30x0.5 mm. The curves exhibit strong fluctuations throughout the frequency band of 0 to 300 kHz. These fluctuations are difficult to be accurately evaluated and therefore, the curves are indicatively fitted by exponential functions, which although do not map the fluctuations, follow the general increasing trend. It is seen that plain mortar exhibits the lowest attenuation, while the attenuation curve of the 10% inclusions is the highest. The inclusions force an attenuation increase of approximately 200% - 300% compared to the attenuation of the plain material, while at the same time they were responsible only for a slight decrease of 35% in Rayleigh velocity, as was seen earlier. Additionally, the curve of 1% damage content is distinctly higher than plain material, showing the strong sensitivity of attenuation even to slight damage content.

As mentioned earlier, apart from the content, the size of the inhomogeneity plays an important role in the wave behavior and especially the attenuation. This is demonstrated in Fig. 7 where the attenuation curves for different sizes of inclusions are shown for the content of 5%. In general all "damaged" material curves exhibit an increase with frequency, as is expected for scattering media in a moderate frequency regime. The inclusions size 30x30x0.2 mm exhibits the highest attenuation in average (approximately 0.016 dB/mm), while 30x30x0.5 mm the lowest of all "damaged" specimens (0.013 dB/mm). The attenuation

curve of sound material is much lower (average at 0.005 dB/mm). This attenuation behavior is a result of the combined effect of geometric spreading, damping and scattering. Geometric spreading has exactly the same effect on all curves, due to the same experimental conditions. Damping depends on the viscosity parameters of the constituents and therefore, for material with the same content of inclusions should not lead to strong changes. Therefore, the strong discrepancies between the curves within the graph, are attributed directly to scattering on the flakey inclusions. The different size of them imposes different scattering conditions and crucially affects the scattered wave field. For certain frequency bands differences of the order of 100% may arise depending on the size of the inclusions alone, even though the inclusion content is constant. This trend once again shows the complexity of wave propagation in damaged concrete and the need of multi-parameter approach for structural condition characterization. In general, it can be mentioned that 30x30x0.5 mm inclusion size exhibits the lowest attenuation curve. This is reasonable since for this shape, the volume of each particle is larger, and therefore, less individual inclusions are necessary to build the specified content. This leads to less scattering incidences as the wave propagates from the excitation point to the receivers, only moderately reducing the amplitude of the wave recorded.

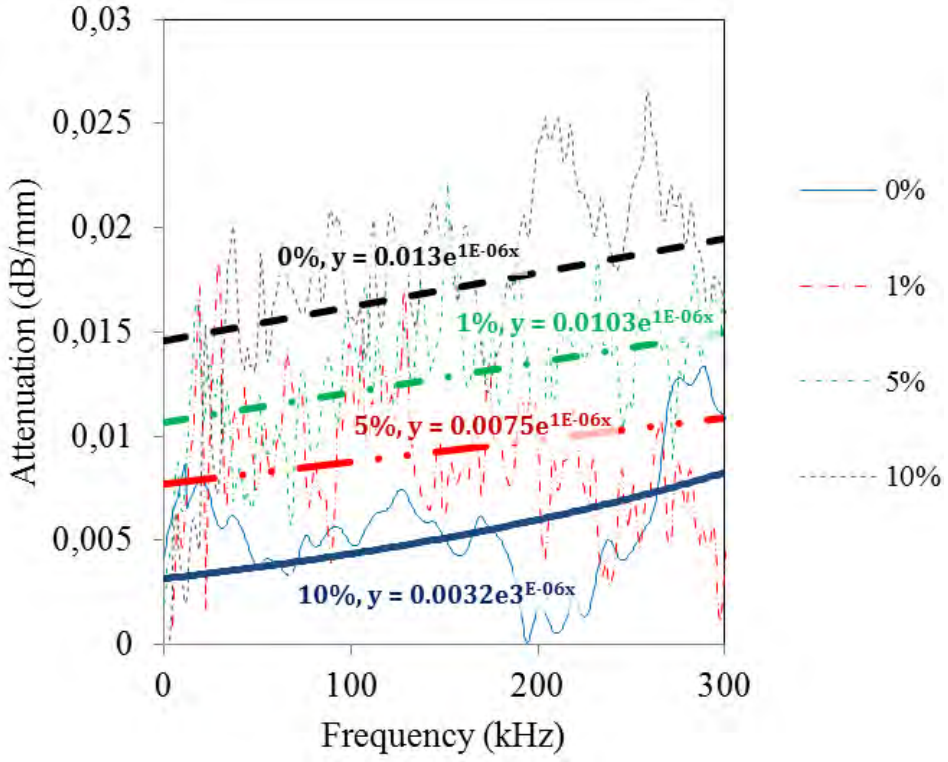

Fig. 6. Attenuation vs. frequency for mortar with different inclusion contents and inclusion size 30x30x0.5 mm.

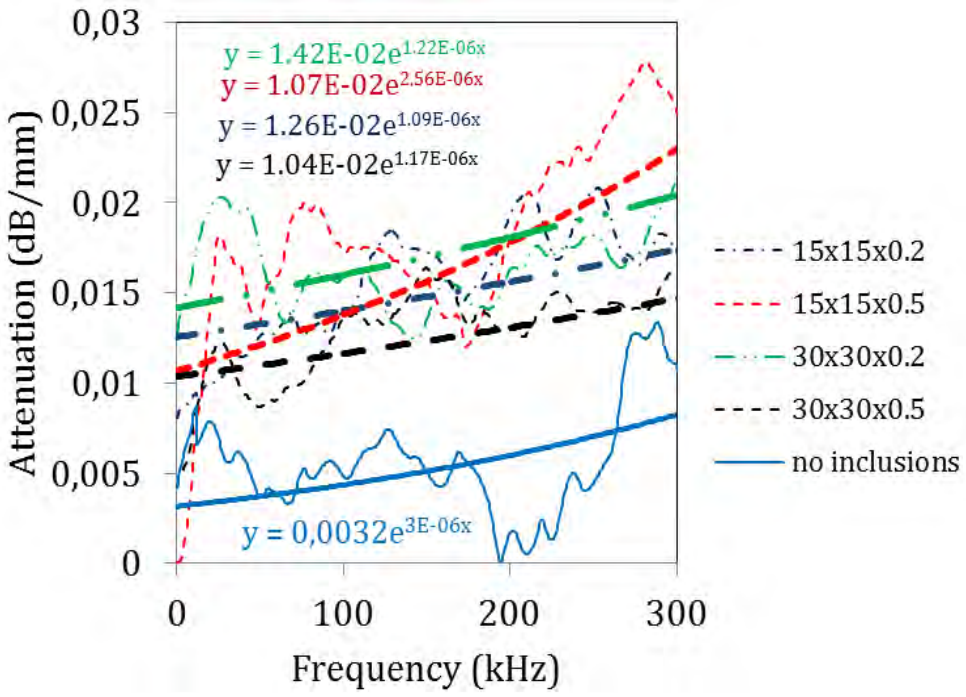

Fig. 7. Attenuation vs. frequency for mortar with different inclusion size and content 5%.

As a conclusion to the study on concrete it is worth to mention that surface wave propagation has not been previously studied for media with randomly distributed inhomogeneity. In this case surface wave features are used for accurate material characterization. Wave velocity of both longitudinal and Rayleigh waves exhibit close connection to the damage content as well as typical size. However, phase velocity vs. frequency curves prove more sensitive since they exhibit stronger decrease for the same damage content. Additionally spectral distortion can also be exploited by means of the coherence function and supply another descriptor sensitive to damage content and size. Finally, attenuation coefficient seems to be the strongest parameter since it suffers an increase of even 300 % compared to sound material. The merit from such a work would be the application of these parameters in real structures, since the complementary use of a combination of parameters will certainly enhance the characterization accomplished by pulse velocity alone.

3. Ultrasonic microscopy for characterization of damage in fiber-reinforced composites

The principle of operation of ultrasonic microscopy is based on the production and propagation of surface acoustic waves (SAW) as a direct result of a combination of the high curvature of the focusing lens of the transducer and the defocus of the transducer into the sample [47, 48]. The most important contrast phenomenon in this technique is based on the

attenuation of Rayleigh waves which are leaking toward the transducer and are very sensitive to local mechanical properties of the materials being evaluated [36]. The generation and propagation of a leaky Rayleigh wave is modulated by the material's properties, thereby making it feasible to image even very subtle changes of the mechanical properties. The sensitivity of the SAW signals to surface and subsurface features depends on the degree of defocus and has been documented in the literature as the V(z) curves [49]. A V(z) curve is obtained when the transducer, kept over a single point, is moved toward the specimen. Then, the signal, rather than simply decreasing monotonically, can undergo a series of oscillations. The series of oscillations at a defocus distance can be associated with Rayleigh wave excitation and interaction of a SAW with the specular reflection received directly by the transducer. The Rayleigh wave velocity, v_R, can then be calculated using a simple relationship:

$$v_R = \frac{v_o}{\sqrt{1 - \frac{v_o}{2\omega\Delta z}}} \tag{3}$$

where, v_o is the sound velocity in the coupling medium, ω is the frequency of ultrasound, and Δz is the periodicity of the V(z) curve.

The defocus distance also has another important effect on the SAW signal obtained by the SAM transducer and dictates whether the SAW signal is separated in time from the specular reflection or interferes with it. Thus, depending on the defocus, the technique can be used either to map the interference phenomenon in the first layer of subsurface fibers, or to map the surface and subsurface features in the sample.

The conventional technique for measuring SAW velocity is based on a V(z) curve acquisition and analysis procedure utilizing a tone-burst system to interrogate the sample at a specific frequency using specially designed acoustic lenses. This technique requires calibration of the specific lens as well as of the response of the electronic circuit using a V(z) curve obtained from a lead sample, a material for which the Rayleigh wave has too low a velocity to be excited. This procedure requires specialized instrumentation, is time-consuming, and cannot be used for on-line measurements in interrupted testing mode. However, a novel ultrasonic microscopy method [37] overcomes the limitations of the conventional technique because it is based on automated SAW velocity determination via V(z) curve measurements using short-pulse ultrasound. The principle of ultrasonic microscopy is presented in Figure 8. A SAM transducer is schematically shown in Figure 1. The transducer used in ultrasonic microscopy has a piezoelectric-active element situated behind a delay line made of fused silica. The thickness of the active element is chosen to excite ultrasonic signals with a desired nominal frequency when an electrical spike voltage is delivered to the piezoelectric element. The silica delay has a highly focused spherical acoustical concave lens that is ground to an optical finish. A numerical aperture (NA; ratio of the diameter of the lens to the focal distance) of >1 (or F number—focal distance/diameter—of the lens <1) is essential for the ultrasonic microscopy technique to effectively generate and receive surface waves [50] in the sample being imaged.

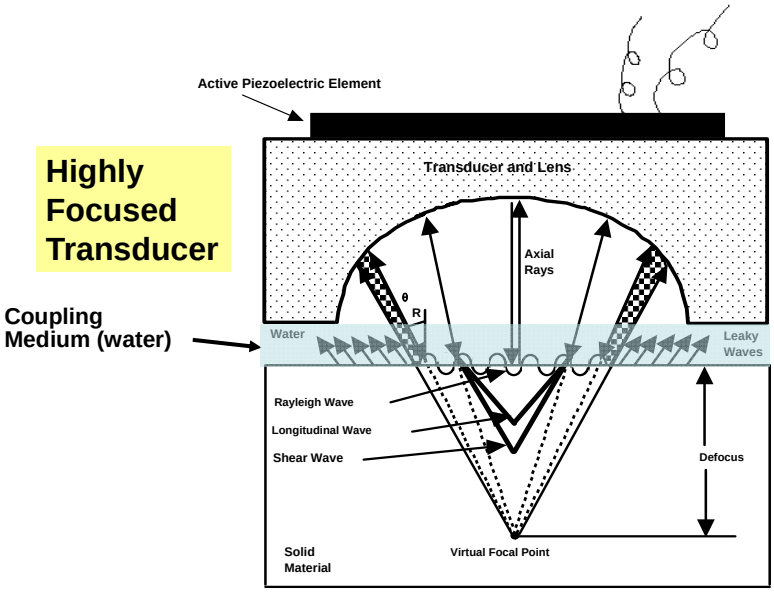

Fig. 8. Principle of ultrasonic microscopy.

The sensor used is a highly focused ultrasonic transducer with a central frequency of 50 MHz. The method employed here is self-calibrated, and is used to obtain Rayleigh velocity maps of the specimen through automated V(z) curve acquisition and analysis [37]. The resolution of the technique for characterizing individual fibers and determining interfacial properties strongly depends on the lens defocus from the surface of the sample. In addition, it should be underlined that the choice of the coupling medium is essential for resolving individual fibers in the composite, since, for a specific ultrasonic transducer with a fixed lens curvature, the generation of Rayleigh waves on the surface of the composite only depends on the sound velocities of the coupling medium and of the material under interrogation. Based on Snell's law, the curvature of a transducer's lens required to generate SAW in a material is given by the relationship,

$$\theta = \sin^{-1}\left(\frac{c_{coupling}}{c_{material}}\right) \tag{4}$$

where, θ is the half-arc of the lens, and $c_{coupling}$ and $c_{material}$ are the ultrasonic velocities of the coupling medium and the material, respectively.

Figure 9 shows ultrasonic microscopy imaging of a Ti-24Al-11Nb/SCS-6 composite subjected to thermo-mechanical fatigue (TMF) using a highly focused 50 MHz transducer, designed to generate SAW in metals such as titanium and steel with water as a coupling medium.

Due to environmental exposure, oxides were formed on the material's surface. This altered the sound velocity of the surface of the composite and, therefore, SAW could not be generated (Fig. 9a). The use of methanol as a coupling medium alleviated this difficulty (Fig. 9b).

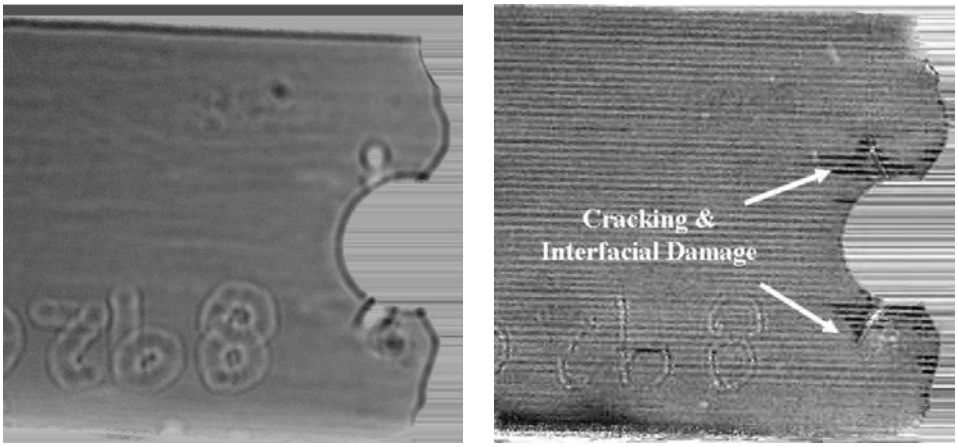

(a) (b)

Fig. 9. The role of coupling medium in ultrasonic microscopy; using (a) water as coupling medium for imaging damage in Ti-24Al-11Nb/SCS-6 composite subjected to TMF, (b) methanol as coupling medium for imaging the same specimen.

The capability of ultrasonic microscopy to determine cracks size and evaluate interfacial damage is depicted in Figure 10. This figure shows the first ply of titanium matrix composites with $[0/90]_S$ cross-ply and unidirectional lay-up of fibers subjected to isothermal mechanical fatigue [51, 52]. Matrix cracks and interfacial debonding are clearly observed in the figure. Crack bridging by unbroken fibers resulting to interface debonding dominate the fatigue crack growth life as evidenced by the characteristic decrease in crack growth rates as the crack length increased during fatigue cycling.

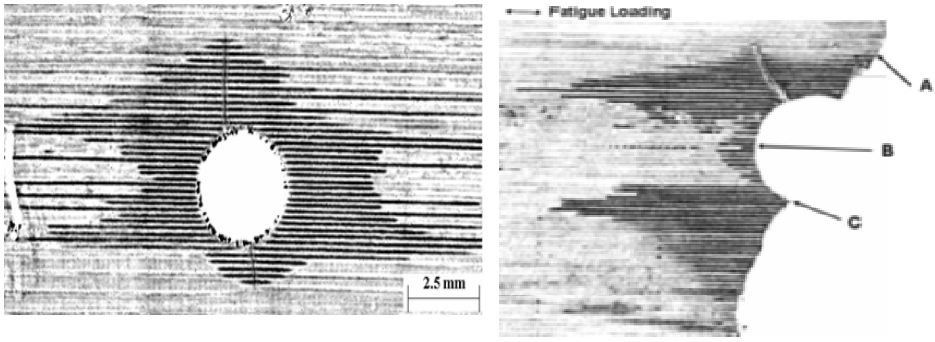

(a) (b)

Fig. 10. Ultrasonic microscopy micrographs of (a) Ti-15Mo-3Nb-3Al-0.2Si/SCS-6 composite with [0/90]S cross-ply lay-up of fibers subjected to 70 hours of isothermal (650^{o}C) fatigue; (b) Ti-15Mo-3Nb-3Al-0.2Si/SCS-6 composite with unidirectional lay-up of fibers after $1.8x10^5$ cycles of isothermal (650^{o} C) fatigue: A. Point of accelerated crack growth to failure. B. Interfacial degradation due to compressive stresses. C. Interfacial degradation due to tensile stresses.

4. Real-time assessment of damage in aerospace materials based on nonlinear surface acoustic waves

This section presents an innovative NDE technique based on nonlinear surface-wave acoustics, which is sensitive to early stages of the fatigue process. A nonlinear parameter is derived and monitored to quantify the state of damage during cyclic loading of the material.

4.1 Background

A reliable inspection methodology for quantifying damage in space structures and for relating the level of damage to the remaining life of the material is essential for preventing catastrophic failures in aerospace systems. Many researchers have tried to develop techniques for fatigue damage characterization of aerospace materials based on linear acoustics, i.e. measurements of ultrasonic velocity and attenuation.

Studies of sound velocity as a function of number of fatigue cycles do not show appreciable changes. On the other hand, ultrasonic attenuation exhibits large changes however, relating these changes to the level of material damage is almost impossible since many other factors (experimental parameters, grain size, etc.) can affect the attenuation in a similar way. Studies [53] on nonlinear property of aluminium alloy and stainless steel have shown dramatic changes in the nonlinearity parameter by the time the material undergoes 30-40% of total fatigue life. However, this technique could not be applied, in real time, in test specimens during fatigue. Several dog-bone fatigue specimens were prepared, then fatigued to different number of cycles and the middle section of each one was cut off. This process is reliable as long as the test coupons are assumed to have the same microstructural characteristics before fatigue. However, due to normal statistical variability of test coupons this methodology may not provide meaningful information about the fatigue process. Moreover, the method is not applicable in real structures for health monitoring purposes. Other studies were carried out [38, 39], where two piezoelectric crystals were placed on the two opposite ends of a dog-bone titanium alloy specimen, and nonlinear measurements were performed in real time on the same specimen while undergoing cyclic loading. These studies utilized bulk acoustic waves and was a first step in the direction of developing a methodology for continuing monitoring of fatigue damage in the laboratory. The main drawback of the method for evaluating damage evolution in real aerospace structures is that it is based on bulk acoustic waves and requires access on the two sides of the structure that must also be perfectly parallel to each other, which is not the usual case. Based on the excellent results that the bulk-wave nonlinear method showed for evaluating the level of damage in aerospace materials, a whole new approach has been developed by performing second harmonic nonlinear measurements of surface acoustic waves, which enabled true health monitoring of damage evolution in space structures since the use of SAW overpasses the limitations of existing methods and do not require access to both sides of the structure.

In order to enhance the understanding and predict fatigue failure in critical components used in aerospace applications an innovative NDE technique based on nonlinear acoustics has been developed. This method is sensitive to early stages of fatigue damage accumulation. Failures of engine components, which often occur much earlier than predictions by initial design, increase the need for reliable NDE methods for early fatigue damage characterization. In order to characterize fatigue mechanisms using acoustic waves

it is necessary to understand the physics of propagation of acoustic or elastic waves in solids and also the physics involved in the process of fatigue damage in materials. In this direction, the "vibrating string model of dislocation damping" developed in the 1950's [54] is the starting point for all the theories on acoustic wave interaction with dislocations.

It is well known that linearized relation between stress and strain "linearized Hooke's law" is sufficient to describe the mechanical properties of solids. The Hooke's law provides a way to relate stress to strain through the second order elastic constants or moduli of the solid. The linear approximation allows the properties of the material that can be measured experimentally to two properties namely, the velocity of sound (elastic modulus) and attenuation (damping) in the material. However, it has been shown [53] that these parameters are not robust enough to describe the fatigue mechanism. Generally a solid possesses nonlinear elastic behavior, but for practical engineering applications and for the purpose of simplification it is ignored and treated as a linear material. Thus it is necessary to understand acoustic wave propagation in nonlinear elastic material. Introduction of nonlinear terms into stress-strain relationship leads to inclusion of higher-order elastic constants.

4.2 Theoretical analysis

Derivation of analytical expressions for the nonlinear parameter enables using nonlinear acoustics techniques for real-time monitoring of fatigue damage accumulation in engineering materials.

4.2.1 Nonlinear bulk-wave propagation

In conventional wave propagation analysis the solid medium is considered as linear. Figure 11 depicts the difference in wave propagation between a linear and nonlinear medium.

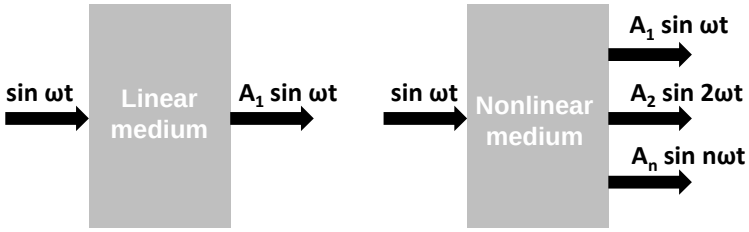

Fig. 11. Linear and nonlinear wave propagation in solid materials.

Engineering materials are nonlinear media. The fundamental wave (sin ωt) that propagates in such material will distort as it propagates, therefore the second-order (sin 2ωt) and higher-order (sin nωt) harmonics will be generated. The anharmonicity of the lattice and dislocation structures contribute in particular to the nonlinearity parameter, β, of the material. This parameter is a measure of the degree of material nonlinearity.

A longitudinal stress, σ, associated with an ultrasonic wave propagating in the material produces a longitudinal strain, ε, which is a combination of elastic, ε_{el}, and plastic, ε_{pl}, strains: $\varepsilon = \varepsilon_{el} + \varepsilon_{pl}$. The plastic strain component is associated with the motion of

dislocation in the dipole configuration [53-55]. The relation between the stress and elastic strain can be written in the nonlinear form of Hooke's law (quadratic nonlinear approach),

$$\sigma = \mathrm{A}_2^e \varepsilon_e + \frac{1}{2}\mathrm{A}_3^e \varepsilon_e^2 + \ldots \text{ or } \varepsilon = \frac{1}{\mathrm{A}_2^e}\sigma - \frac{1}{2}\frac{\mathrm{A}_3^e}{\left(\mathrm{A}_2^e\right)^3}\sigma^2 + \ldots \tag{5}$$

where A_2^e and A_3^e are the Huang coefficients.

By considering the dipolar forces one can easily obtain the relation between the stress and the plastic strain [53]. For edge dislocation pairs with opposite polarity, for example, these forces can be written in the following form:

$$F_x = -\frac{Gb^2}{2\pi(1-\nu)}\frac{x\left(x^2-y^2\right)}{\left(x^2+y^2\right)^2} \tag{6}$$

where, b is the Burgers vector, v the Poisson's ratio, G the shear modulus, and x and y the Cartesian coordinates of one dislocation in the pair in respect to the other. At equilibrium state, y equals the dipole height, h.

The relation between the plastic strain and the relative dislocation displacement ξ=x−h is given by the expression $\varepsilon_{pl} = \Omega\Lambda_{dp} b\xi$, where Ω is a conversion factor and Λ_{dp} is the dipole density [53].

Using these relationships and an expansion of Eq. (6) in a power series in x with respect to h leads to the following equation

$$\sigma = \mathrm{A}_2^e\left[\varepsilon - \frac{1}{2}\left(\frac{\mathrm{A}_3^e}{\left(\mathrm{A}_2^e\right)^3} + \frac{\mathrm{A}_3^{dp}}{\left(\mathrm{A}_2^{dp}\right)^3}\right)\right]\varepsilon^2 + \ldots \tag{7}$$

The wave equation with respect to the Lagrangian coordinate X is given by

$$\rho\frac{\partial^2\varepsilon}{\partial t^2} = \frac{\partial^2\sigma}{\partial \mathrm{X}^2} \tag{8}$$

Replacing σ, given by Eq. (7), in Eq. (8) the following equation can be obtained:

$$\frac{\partial^2\varepsilon}{\partial t^2} - c^2\frac{\partial^2\varepsilon}{\partial \mathrm{X}^2} = -c^2\beta\left[\varepsilon\frac{\partial^2\varepsilon}{\partial \mathrm{X}^2} + \left(\frac{\partial\varepsilon}{\partial X}\right)^2\right] \tag{9}$$

where $c = \sqrt{\frac{A_2^e}{\rho}}$ and $\beta = \beta_e + \beta_{dp}$ with $\beta_e = -\frac{A_3^e}{A_2^e}$ and $\beta_{dp} = \frac{16\pi\Omega R^2\Lambda_{dp}h^3(1-\nu)^2\left(\mathrm{A}_2^e\right)^2}{G^2 b}$

The Huang coefficients can be expressed in terms of higher elastic constants. Specifically,

$A_1^e = C_1$ (C_1 equals the initial stress)

$A_2^e = C_1 + C_{11}$

$A_3^e = 3C_{11} + C_{111}$

Assuming $C_1 = 0$, the portion of β describing the nonlinear contribution from the elasticity of the lattice can be written in the form, $\beta_e = -\left(3 + \frac{C_{111}}{C_{11}}\right)$.

Assuming a purely sinusoidal input wave, $\varepsilon_o \sin(\omega t - kX)$, a solution to Eq. (9) is:

$$\varepsilon = \varepsilon_o \sin(\omega t - kX) - \frac{1}{4}\beta k \varepsilon_o^2 X \sin\left[2(\omega t - kX)\right] \tag{10}$$

Therefore β can be described by the following expression containing the amplitudes of the fundamental wave, A_1, and the second harmonic, A_2,

$$\beta = \frac{4k}{X}\frac{A_2}{A_1^2} \tag{11}$$

Eq. (11) permits the experimental determination of the nonlinear parameter β. This parameter depends on the amplitudes of the fundamental as well as the second harmonic, the frequency, wave velocity and propagation distance. To obtain experimentally the nonlinear parameter β of a material, the amplitude of the second harmonic needs to be determined experimentally using a specific frequency and propagation distance (38-40,53).

4.2.2 Nonlinear Rayleigh wave propagation

The analysis for obtaining β as described in Section 4.1.1 is only valid for longitudinal ultrasonic waves. The derivation of the nonlinear parameter β for the propagation of 2-D Rayleigh waves is more challenging. Surface acoustic waves are in general a superposition of bulk waves. Longitudinal waves are sensitive as it concerns the generation of higher harmonics, contrary to shear waves which are not considered prone to higher harmonic generation. In this respect, Rayleigh waves are expected to have a similar nonlinear wave propagation behavior as the longitudinal waves. In practice, it is essential to derive the nonlinear parameter β for surface acoustic waves as a function of the amplitudes of the fundamental frequency and the second order harmonic.

If one considers a Rayleigh wave propagating in the positive x direction, assuming the z axis into the material, the displacement potentials describing the longitudinal and shear ultrasonic waves,

$$\varphi = Ae^{-k\sqrt{1-\left(\frac{c}{c_L}\right)^2}z}e^{ik(x-ct)} \tag{12}$$

$\phi = Be^{-k\sqrt{1-\left(\frac{c}{c_S}\right)^2}z} e^{ik(x-ct)}$ can be re-written in the form:

$$\varphi = -i\frac{B_1}{k_R} e^{-\sqrt{k_R^2-k_l^2}z} e^{i(k_R x-\omega t)} \tag{13}$$

$$\phi = -i\frac{C_1}{k_R} e^{-\sqrt{k_R^2-k_S^2}z} e^{i(k_R x-\omega t)}$$

where, k_R, k_l, k_s are the wave-numbers for Rayleigh, longitudinal, and shear ultrasonic waves, respectively [56].

Considering the boundary conditions for a stress-free surface in Eq. (13), a relation between the constants B_1 and C_1 can be obtained:

$$B_1 = -i\frac{2k_R\sqrt{k_R^2-k_1^2}}{2k_R^2-k_S^2}C_1 \tag{14}$$

Taking into account that the surface acoustic waves are a superposition of longitudinal and shear waves propagating along a stress-free surface that have the same velocity, the displacement components can be decomposed into their longitudinal and shear components [56-60]:

$$u_x = B_1\left(e^{-\sqrt{k_R^2-k_l^2}z} - \frac{2\sqrt{\left(k_R^2-k_l^2\right)\left(k_R^2-k_S^2\right)}}{2k_R^2-k_S^2} e^{-\sqrt{k_R^2-k_S^2}z}\right) e^{i(k_R x-\omega t)} \tag{15}$$

$$u_z = iB_1\frac{\sqrt{k_R^2-k_l^2}}{k_R}\left(e^{-\sqrt{k_R^2-k_l^2}z} - \frac{2k_R^2}{2k_R^2-k_S^2} e^{-\sqrt{k_R^2-k_S^2}z}\right) e^{i(k_R x-\omega t)}$$

The first term in Eq. (15a) presents the pure longitudinal wave motion. Considering a material with a weak nonlinearity, the second order harmonic Rayleigh waves that propagate a large enough distance can be expressed in the form [56-60]:

$$u_x \approx B_2\left(e^{-2\sqrt{k_R^2-k_l^2}z} - \frac{2\sqrt{\left(k_R^2-k_l^2\right)\left(k_R^2-k_S^2\right)}}{2k_R^2-k_S^2} e^{-2\sqrt{k_R^2-k_S^2}z}\right) e^{i2(k_R x-\omega t)} \tag{16}$$

$$u_z \approx iB_2\frac{\sqrt{k_R^2-k_l^2}}{k_R}\left(e^{-2\sqrt{k_R^2-k_l^2}z} - \frac{2k_R^2}{2k_R^2-k_S^2} e^{-2\sqrt{k_R^2-k_S^2}z}\right) e^{i2(k_R x-\omega t)}$$

Taking into account the fact that the acoustic nonlinear behavior of the shear waves in an isotropic medium ceases to exist due to the symmetry of the third order elastic constants, it can be inferred that the longitudinal wave component is only one contributing to the higher

harmonic generation in the case of the propagation of surface acoustic waves. Hence, the amplitudes of the in-plane displacement, u_x, of the fundamental and second harmonic of a near-surface Rayleigh wave can be related as those in the case of bulk longitudinal waves [56]:

$$B_2 = \frac{\beta k_1^2 x B_1^2}{8} \tag{17}$$

where β is the acoustic nonlinear parameter for the bulk longitudinal waves, and x is the propagation distance.

In case of experimental determination of β for Rayleigh waves using contact ultrasonic transducers of interferometry, the out-of-plane component on the surface (z=0) of the particle velocity, $\overline{u}_z$ or displacement, u_z, is detected.

From Eqs. (15b), (16b), and (17), the ratio of the amplitudes of the second harmonic to the fundamental is given by:

$$\frac{\overline{u}_z(2\omega)}{\overline{u}_z^2(2\omega)} = \frac{\beta k_1^2 x}{8i\left(\frac{\sqrt{k_R^2 - k_l^2}}{k_R}\right)\left(1 - \frac{2k_R^2}{2k_R^2 - k_S^2}\right)} \tag{18}$$

where $\overline{u}_z(\omega) = u_z(\omega; x, z=0)$. Therefore, the measured out-of-plane displacement components are related to the acoustic nonlinear parameter β for the bulk longitudinal waves [56],

$$\beta = \frac{8i\ \overline{u}_z(2\omega)}{k_l^2 x\ \overline{u}_z^2(\omega) k_R} \frac{\sqrt{k_R^2 - k_l^2}}{k_R}\left(1 - \frac{2k_R^2}{2k_R^2 - k_S^2}\right) \tag{19}$$

While the shear wave alone does not generate higher harmonics, shear wave components interact with longitudinal ones, as it becomes evident from the second term in the parenthesis of Eq. (19).

The harmonic ratio $\frac{\overline{u}_z(2\omega)}{\overline{u}_z^2(\omega)} \approx \frac{A_2}{A_1^2}$ can be used to determine material nonlinearity and to assess the state of damage in materials with different levels of fatigue. The dimensionless nonlinear parameter β in case of propagating Rayleigh surface waves in the material is also dependent on the amplitude ratio $\frac{A_2}{A_1^2}$ as in case of bulk longitudinal waves.

Although the nonlinear parameter β remains constant for different propagation distances, the amplitude of the second harmonic changes linearly with the propagation distance, as required for a quadratic nonlinearity [56].

4.3 Real time measurement of material nonlinearity during fatigue

In the measurement of nonlinearity parameter β under cyclic loading the change in β is more important than its absolute values. Hence, measurements of relative changes in the

nonlinearity of the material from the virgin state to a fatigued state are discussed here. Therefore, the β parameter defined in Eq. (19) and normalized by the value β_o (nonlinear parameter of the material at the virgin state) is experimentally measured. In this sense, in order to assess the level of fatigue damage using nonlinear acoustics measurements a determination of the absolute value of the material's nonlinearity is not required, enabling real-time experiments [38-39].

Below it is shown an example of assessing in real-time the state of fatigue damage in titanium alloys undergone cyclic loading. The piezoelectric detection of second harmonic ultrasonic amplitude is based on propagating a pure single frequency f ultrasonic wave through the sample. As the elastic wave propagates through the medium, it is distorted as the result of the anharmonicity of the crystalline lattice and other microstructural disturbances, such as the grain boundaries and dislocations. During the fatigue process of Ti-6Al-4V, the lattice anharmonicity remains constant since the stress level applied to the specimen is far below the yield strength i.e., in the elastic region. However, the other factors like grain boundaries, dislocations, and other impurities change as a function of fatigue level. The distorted signal is composed of the combination of the harmonics and grows as it propagates until the attenuation factor stops its growth. The harmonic portion of the distorted ultrasonic signal is very sensitive to the changes in the strain energy density due to the changes of these factors. The second harmonic wave, of frequency 2f, is detected by a second piezoelectric transducer. The transducer was manufactured using 36^o Y-cut $LiNbO_3$ crystals placed inside specially designed brass housing and plexiglass tubing. Lithium niobate single-crystals were used since they are linear materials and also exhibit higher electromechanical coupling compared to quartz crystals.

An important issue for correctly measuring material nonlinearity is to use linear instrumentation. The experimental data shown below are obtained using amplifiers and filters of linear response. For example, the fundamental and second harmonic signals were detected using high quality linear band-pass filters with a rejection ratio better than 60 dB. Two such low power (up to 100 W) filters were designed, one with a central frequency of 5 MHz, the other 10 MHz. Figures 12(a) and 12(b) show the 5 MHz and 10MHz low power filters' characteristics and simulation performance data, respectively.

Transducer holder and the grips for the fatigue load frame were designed to enable on-line monitoring of the material's nonlinearity parameter during the fatigue process, since the conventional grips are inadequate for attaching transducers to the specimen.

The experimental configuration for on-line piezoelectric detection of second harmonic signal during mechanical fatigue is based on a tone-burst generator and a power amplifier to launch longitudinal sound waves into the specimen at a frequency of 5 MHz. A linear high-power band-pass filter was placed between the power amplifier and the transducer to make sure that unwanted harmonic signals are filtered out. The same transducer was used to detect the fundamental signal reflected from the other end of the specimen. A 10 MHz transducer bonded to the other end of the specimen was used to receive the second harmonic signal. After the second harmonic signal is detected, it was fed to a linear narrow band amplifier through the 10 MHz band-pass filter. Both fundamental V_1 (mV) and second harmonic V_2 (mV) signals were sent to the A/D converter for digitization and the nonlinear parameter β was finally determined from the sampled signals.

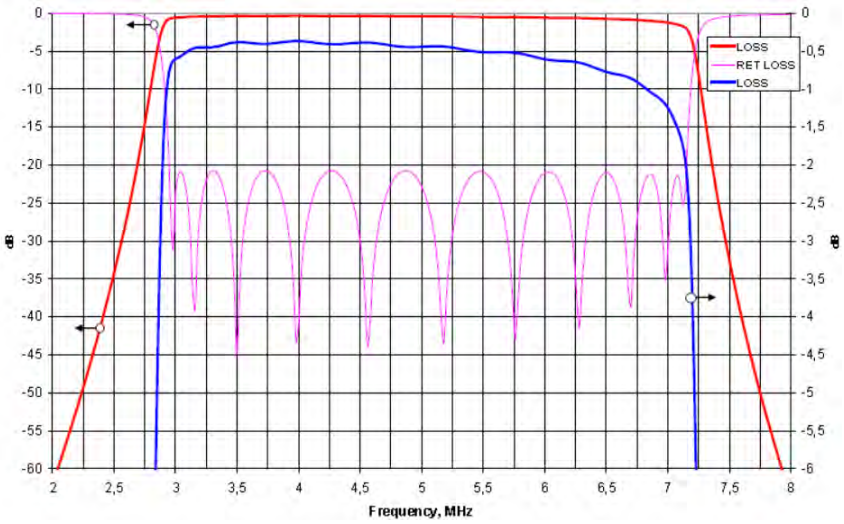

(a)

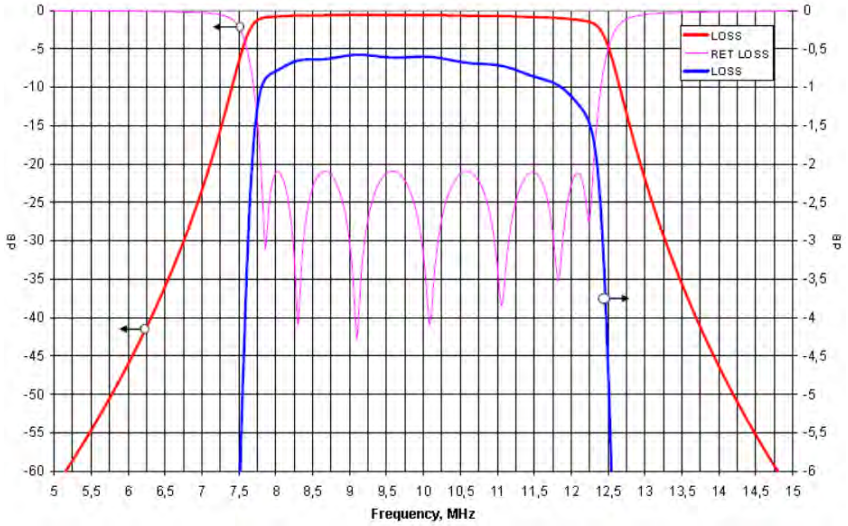

(b)

Fig. 12. Performance data of the (a) 5 MHz and (b) 10 MHz 100 W band-pass filters.

Since the nonlinear property of the specimen was measured, it was necessary to verify that the measurement setup itself was linear indeed. For checking the system's linearity a simple experiment was performed with an unfatigued Ti-6Al-4V sample at room temperature by changing the input voltage to the transmitting transducer. It was thus demonstrated that the slope of the curve of the amplitude of second harmonic vs. the fundamental using the linear filters was linear.

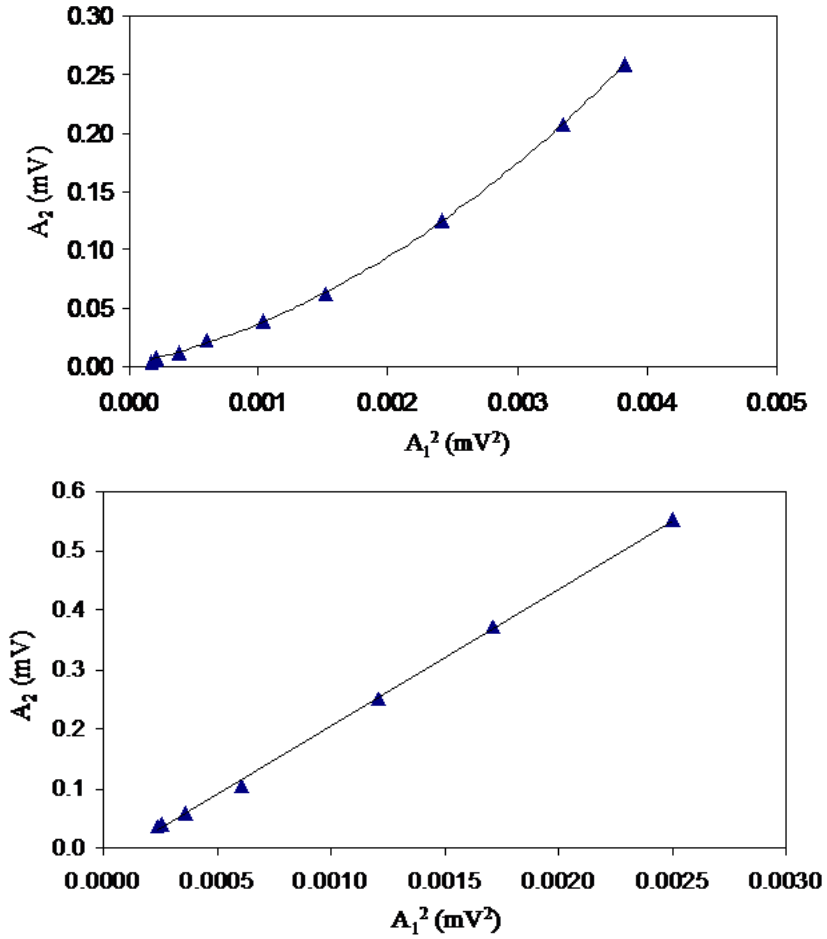

Fig. 13. Linearity check of the measurement setup; (a) without the linear band-pass filter for the second harmonic signal, and (b) with the linear band-pass filter for the second harmonic signal.

As it is demonstrated by comparing Figs. 13(a) and 13(b), using linear band-pass filters leads to a totally linear experimental setup. Thus, any determination of nonlinear behavior can be attributed to material nonlinearity and not to the measurement system.

Since the measurements require a relatively long time for experiments performed at a cyclic frequency of 1 Hz, it is necessary to check the stability of the measuring system over a period time. The amplitudes of the fundamental and second harmonic signals were monitored over a period of 24 hours in the laboratory and only small, almost negligible fluctuations, compared to the size of the measured values during the fatigue test, were observed. Figure 14 shows the amplitudes of the fundamental, A_1, and second harmonic, A_2, signals as a function of time for period of 24 hours in laboratory conditions.

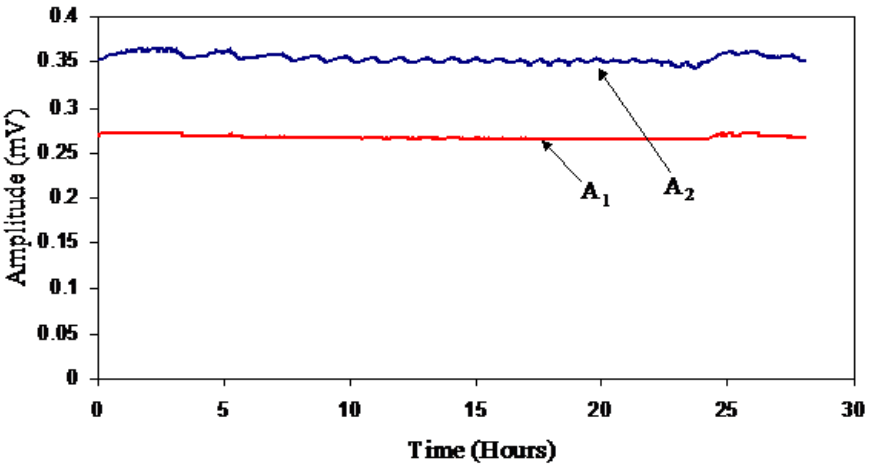

Fig. 14. Long term stability test of the measurement system at room temperature.

The experimental technique described above was used to measure the nonlinear acoustic properties of Ti-6Al-4V alloys and characterize in real-time their fatigue behavior. During the fatigue tests, the samples were subjected to cyclic loading at the frequency of 1 Hz under low cycle fatigue conditions (σ_{max} = 850 MPa, and R ratio = 0.1). The ultrasonic velocity and nonlinear property were measured at zero-load on the sample, at an interval of 100 cycles of fatigue.

Attenuation and velocity of longitudinal wave measurements were performed at a frequency of 5 MHz at various stages of fatigue. It was observed that the longitudinal sound velocity had a minute measurable change in the beginning of the fatigue process (Fig. 15). This can be explained by the small increase of the specimen's length that occurs during the fatigue process. For an accurate determination of the velocity of sound it is necessary to incorporate the changes in the specimen length.

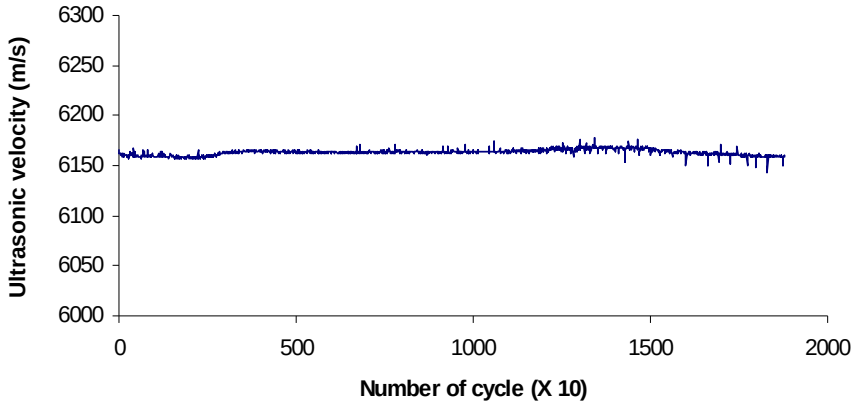

Fig. 15. Variation of longitudinal wave velocity with fatigue life

Additionally, it was observed that the attenuation increased significantly in the initial stages of fatigue (Fig. 16). The initial increase of attenuation of 50 % is quite significant; however, it is less sensitive to fatigue process beyond 20% of the fatigue life. The higher attenuation at the higher fatigue cycles may indicate an increase in the scattering of sound waves due to the increased dislocation dipole density from fatigue. As the increase in dislocation density saturates, the level of scattering of sound wave within the material become stable. It should be pointed out, however, that the general tendency of dislocation movement is known to migrate to the surface of the material. This could mean that the attenuation measurement in the bulk is less meaningful throughout the entire lifetime of the material.

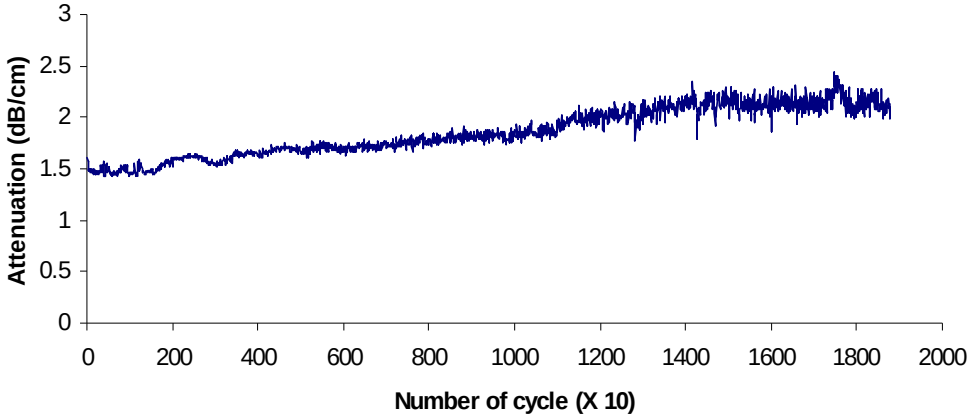

Fig. 16. Variation of ultrasonic attenuation with fatigue life

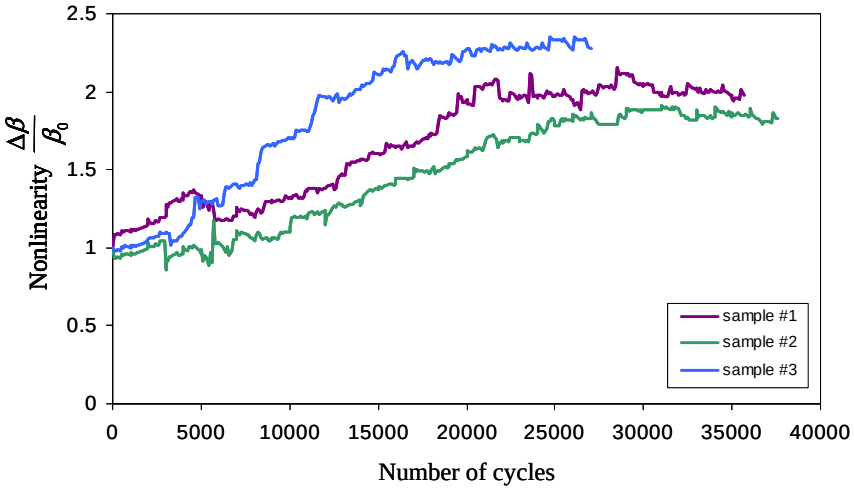

Fig. 17. Variation of the nonlinear parameter β with fatigue life in Ti-6Al-4V

Variation in amplitude of the second harmonic signal, as the amplitude of the fundamental signal is changed, was used for measurement of nonlinear acoustic behavior of the material.

As the material was undergoing fatigue the amplitude of the second harmonic signal increases to give a steeper slope. Figure 17 shows measurements of β as a function of fatigue cycles for three different Ti-6Al-4V samples. The trend of the variation of relative β as a function of fatigue life is similar for the three samples; however, the level of nonlinearity is different due to the fact that different samples are fatigue damaged in a dissimilar way.

Figure 18 depicts the normalized nonlinearity (shown with line plot) of Ti-6Al-4V samples as a function of the number of cycles and correlation with transmission electron microscopy (TEM) analysis of the dislocation density (shown with data points). It can be observed in Fig. 18 that acoustic nonlinearity of the material exhibits large changes during the fatigue process. This finding is in contrast with the measurements of attenuation and elastic behavior, where the majority of variation occurred before the 20% of fatigue lifetime. The second harmonic signal generated during the fatigue process is not only sensitive to the early stage of the process, but also to later stages of damage. This implies that the harmonic signal is very sensitive to the microstructural changes in the material. The variation of nonlinearity continues due to the generation of additional dislocation dipoles by the fatigue process and their interaction with the acoustic waves, as predicted by relevant models and experimental work [38-40, 53].

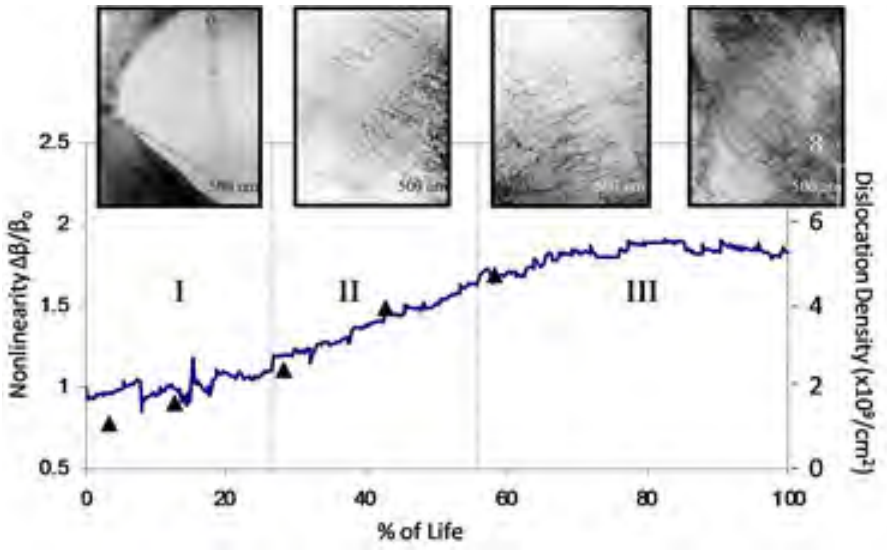

Fig. 18. Correlation of TEM imaging and dislocation density in Ti-6Al-4V with normalized nonlinearity as a function of fatigue level.

5. Conclusion

The present chapter gives an overview of contemporary techniques to assess the quality of materials using surface elastic waves. It is highlighted that different instrumentation and methodology facilitates non destructive evaluation in quite distinct material groups, like concrete and aerospace composites. In both kinds of material, damage is primarily initiated on the surface. Therefore, early assessment by surface waves is crucial for the estimation of

remaining life or repair method. Concrete, including large scale of inhomogeneity is typically examined by comparatively long wavelengths by means of pulse velocity correlation with strength or damage. The present study complements the information of pulse velocity using features like the dispersion curve, the attenuation coefficient as a function of frequency, as well as the spectral distortion between pulses recorded at different points of the surface. It is seen that combined wave features can act complementary, while their acquisition does not require further upgrade on the equipment used for conventional pulse velocity measurements. Concerning alloys and metal matrix composites used in aerospace applications, due to their much shorter typical size of inhomogeneity, delicate equipment should be employed enabling the evaluation on a microscopic scale. In these components fatigue loading is of primary concern, which may result in different damage modes. Acoustic microscopy enables the scanning of the material for surface or subsurface defects providing a detailed point by point assessment on the elastic properties. Additionally, nonlinear surface waves are extremely sensitive to the evolution of micro-damage, including dislocation motion and micro-cracking. This is due to the development of higher harmonics and, therefore, is an excellent way to monitor in real time the damage as evolved during cyclic loading from early stages of fatigue to final failure of the structure. The derived nonlinear parameter enables the prediction of remaining life in critical components.

6. References

[1] Kaplan, M. F. (1959). The Effects of Age and Water/Cement Ratio Upon the Relation between Ultrasonic Pulse Velocity and Compressive Strength. *Mag. Concrete Res.,* Vol. 11, No. 32, pp. 85-92

[2] Popovics, S., Rose, J. L. and Popovics, J. S. (1990). The Behavior of Ultrasonic Pulses in Concrete. *Cement Concrete Res.,* Vol. 20, pp. 259–270

[3] Qixian, L. and Bungey, J. H. (1996). Using Compression Wave Ultrasonic Transducers to Measure the Velocity of Surface Waves and Hence Determine Dynamic Modulus of Elasticity for Concrete. *Constr Build Mater,* Vol. 4, pp. 237–242

[4] Graff, K. F. (1975). Wave Motion in Elastic Solids. *New York: Dover Publications,* Vol., No.

[5] Philippidis, T. P. and Aggelis, D. G. (2005). Experimental Study of Wave Dispersion and Attenuation in Concrete. Ultrasonics. 43, No. 7, pp. 584-595

[6] Kinra, V. K. and Rousseau, C. (1987). Acoustical and Optical Branches of Wave Propagation. *J.Wave-Mater. Interact.,* Vol. 2, pp. 141–152

[7] Sachse, W. and Pao, Y.-H. (1978). On the Determination of Phase and Group Velocities of Dispersive Waves in Solids. *J. Appl. Phys.,* Vol. 49, No. 8, pp. 4320–4327

[8] Aggelis, D. G. and Shiotani, T. (2007). Experimental Study of Surface Wave Propagation in Strongly Heterogeneous Media. *Journal of the Acoustical Society of America,* Vol. 122, No. 5, pp. EL 151-157

[9] Washer, G. A., Green, R. E. and Jr, R. B. P. (2002). Velocity Constants for Ultrasonic Stress Measurement in Prestressing Tendons. *Res. Nondestr. Eval.,* Vol. 14, pp. 81-94

[10] Cowan, M. L., Beaty, K., Page, J. H., Zhengyou, L. and Sheng, P. (1998). Group Velocity of Acoustic Waves in Strongly Scattering Media: Dependence on the Volume Fraction of Scatterers. *Phys. Rev. E,* Vol. 58, pp. 6626–6636

[11] Sansalone, M. and Carino, N. J. (2004). Stress Wave Propagation Methods. *CRC Handbook on Nondestructive Testing of Concrete, Malhotra V. M., Carino N. J., eds. CRC Press, Boca Raton FL,* pp. 275-304

[12] Naik, T. R., Malhotra, V. M. and Popovics, J. S. (2004). The Ultrasonic Pulse Velocity Method. *Malhotra VM, Carino NJ. editors. CRC Handbook on nondestructive testing of concrete. Boca Raton: CRC Press*

[13] Philippidis, T. P. and Aggelis, D. G. (2003). An Acousto-Ultrasonic Approach for the Determination of Water-to-Cement Ratio in Concrete. *Cement and Concrete Research,* Vol. 33, No. 4, pp. 525-538

[14] Gudra, T. and Stawinski, B. (2000). Non-Destructive Characterization of Concrete Using Surface Waves. *NDT&E INT,* Vol. 33, pp. 1-6

[15] Aggelis, D. G., Kordatos, E. Z., Strantza, M., Soulioti, D. V. and Matikas, T. E. (2011). NDT Approach for Characterization of Subsurface Cracks in Concrete. *Construction and Building Materials,* Vol. 25, pp. 3089-3097

[16] Aggelis, D. G. and Shiotani, T. (2008). Surface Wave Dispersion in Cement-Based Media: Inclusion Size Effect. *NDT&E INT,* Vol. 41, pp. 319-325

[17] Landis, E. N. and Shah, S. P. (1995). Frequency-Dependent Stress Wave Attenuation in Cement-Based Materials. *J. Eng. Mech.-ASCE,* Vol. 121, No. 6, pp. 737-743

[18] Punurai, W., Jarzynski, J., Qu, J., Kurtis, K. E. and Jacobs, L. J. (2006). Characterization of Entrained Air Voids in Cement Paste with Scattered Ultrasound. *NDT&E International,* Vol. 39, pp. 514–524

[19] Shah, S. P., Popovics, J. S., Subramanian, K. V. and Aldea, C. M. (2000). New Directions in Concrete Health Monitoring Technology. *J. Eng. Mech.-ASCE,* Vol. 126, No. 7, pp. 754-760

[20] Selleck, S. F., Landis, E. N., Peterson, M. L., Shah, S. P. and Achenbach, J. D. (1998). Ultrasonic Investigation of Concrete with Distributed Damage. *ACI Materials Journal* Vol. 95, No. 1, pp. 27-36

[21] Jacobs, L. J. and Owino, J. O. (2000). Effect of Aggregate Size on Attenuation of Rayleigh Surface Waves in Cement-Based Materials. *J. Eng. Mech.-ASCE,* Vol. 126, No. 11, pp. 1124-1130

[22] Owino, J. O. and Jacobs, L. J. (1999). Attenuation Measurements in Cement-Based Materials Using Laser Ultrasonics. *J. Eng. Mech.-ASCE,* Vol. 125, No. 6, pp. 637-647

[23] Aggelis, D. G. (2010). Damage Characterization of Inhomogeneous Materials: Experiments and Numerical Simulatios of Wave Propagation. *Strain,* in press (10.1111/j.1475-1305.2009.00721.x)

[24] Chaix, J. F., Garnie, r. V. and Corneloup, G. (2006). Ultrasonic Wave Propagation in Hetero- Geneous Solid Media: Theoretical Analysis and Experimental Validation. *Ultrasonics,* Vol. 44, pp. 200-210

[25] Kim, D. S., Seo, W. S. and Lee, K. M. (2006). IE–SASW Method for Nondestructive Evaluation of Concrete Structure. *NDT&E International,* Vol. 39, pp. 143-154

[26] Hevin, G., Abraham, O., Pedersen, H. A. and Campillo, M. (1998). Characterisation of Surface Cracks with Rayleigh Waves: A Numerical Model. *NDT&E Int* Vol. 31, No. 4, pp. 289–297

[27] Aggelis, D. G., Shiotani, T. and Polyzos, D. (2009). Characterization of Surface Crack Depth and Repair Evaluation Using Rayleigh Waves. *Cement and Concrete Composites,* Vol. 31, No. 1, pp. 77-83

[28] vanWijk, K., Komatitsch, D., Scales, J. A. and Tromp, J. (2004). Analysis of Strong Scattering at the Micro-Scale. *J. Acoust. Soc. Am.,* Vol. 115, pp. 1006–1011

[29] Pecorari, C. (1998). Rayleigh Wave Dispersion Due to a Distribution of Semi-Elliptical Surface-Breaking Cracks. *J Acoust Soc Am,* Vol. 103, No. 3, pp. 1383-1387

[30] Harmon, D. and Saff, C. (1988). Metal Matrix Composites: Testing, Analysis, and Failure Modes. *Johnson EWS, editor. Damage Initiation and Growth in Fiber Reinforced Metal Matrix Composites. Philadelphia, PA,* Vol. ASTM STP 1032, pp. 237-250

[31] Marshall, D. B., Cox, B. N. and Evans, A. G. (1985). The Mechanics of Matrix Cracking in Brittle-Matrix Fiber Composites. *Acta Metallurgica,* Vol. 33, No. 11, pp. 2013-2021

[32] McCartney, L. N. (1987). Mechanics of Matrix Cracking in Brittle-Matrix Fibre-Reinforced Composites. *Proc. R. Soc. Lond.,* pp. A409:329-350

[33] Karpur, P., Matikas, T. E., Krishnamurthy, S. and Ashbaugh, N. (1992). Ultrasound for Fiber Fragmentation Size Determination to Characterize Load Transfer Behavior of Matrix-Fiber Interface in Metal Matrix Composites. *Thompson DO, Chimenti DE, editors. Review of Progress in Quantitative NDE. La Jolla CA,* Vol. 12B, pp. 1507-1513

[34] Matikas, T. E. (2008). High Temperature Fiber Fragmentation Characteristics of SiC Single-Fiber Composite with Titanium Matrices. *Advanced Composite Materials,* Vol. 17, No. 1, pp. 75-87

[35] Matikas, T. E. and Karpur, P. (1992). Matrix-Fiber Interface Characterization in Metal Matrix Composites Using Ultrasonic Shear-Wave Back-Reflection Coefficient Technique. *Thompson DO, Chimenti DE, editors. Review of Progress in Quantitative NDE. La Jolla CA,* Vol. 12B, pp. 1515-1522

[36] Matikas, T. E., Rousseau, M. and Gatignol, P. (1993). Theoretical Analysis for the Reflection of a Focused Ultrasonic Beam from a Fluid-Solid Interface. *Journal of the Acoustical Society of America,* Vol. 93, No. 3, pp. 1407-1416

[37] Matikas, T. E. (2000). Quantitative Short-Pulse Acoustic Microscopy and Application to Materials Characterization. *Microsc. Microanal.,* Vol. 6, pp. 59–67

[38] Frouin, J., Sathish, S., Matikas, T. E. and Na, J. K. (1999). Ultrasonic Linear and Nonlinear Behavior of Fatigued Ti-6Al-4V. *Journal of Materials Research,* Vol. 14, No. 4, pp. 1295-1298

[39] Frouin, J., Maurer, J., Sathish, S., Eylon, D., Na, J. K. and Matikas, T. E. (2000). Real-Time Monitoring of Acoustic Linear and Nonlinear Behavior of Titanium Alloys During Cyclic Loading. *Nondestructive Methods for Materials Characterization, Materials Research Society,* Vol. 591, pp. 79-84

[40] Matikas, T. E. (2010). Damage Characterization and Real-Time Health Monitoring of Aerospace Materials Using Innovative NDE Tools. *Journal of Materials Engineering and Performance,* Vol. 19, No. 5, pp. 751-760

[41] Aggelis, D. G. and Shiotani, T. (2008). Effect of Inhomogeneity Parameters on the Wave Propagation in Cementitious Materials. *American Concrete Institute Materials Journal,* Vol. 105, No. 2, pp. 187-193

[42] Dokun, O. D., Jacobs, L. J. and Haj-Ali, R. M. (2000). Ultrasonic Monitoring of Material Degradation in FRP Composites. *J. Eng. Mech.,* Vol. 126, pp. 704–710

[43] Aggelis, D. G., Tsinopoulos, S. V. and Polyzos, D. (2004). An Iterative Effective Medium Approximation (Iema) for Wave Dispersion and Attenuation Predictions in Particulate Composites, Suspensions and Emulsions *Journal of the Acoustical Society of America,* Vol. 116, pp. 3443-3452

[44] Mobley, J., Waters, K. R., Hall, C. H., Marsh, J. N., Hughes, M. S., Brandenburger, G. H. and Miller, J. G. (1999). Measurements and Predictions of Phase Velocity and Attenuation Coefficient in Suspensions of Elastic Microspheres. *J. Acoust. Soc. Am.,* Vol. 106, pp. 652-659

[45] Bendat, J. S. and Piersol, A. G. (1993). Engineering Applications of Correlation and Spectral Analysis. *2nd ed., Wiley, New York*

[46] Grosse, C., Reinhardt, H. and Dahm, T. (1997). Localization and Classification of Fracture Types in Concrete with Quantitative Acoustic Emission Measurement Techniques. *NDT&E INT,* Vol. 30, No. 4, pp. 223-230

[47] Quate, C. F., Atalar, A. and Wickramasinghe, H. K. (1979). Acoustic Microscopy with Mechanical Scanning - a Review. *Proceedings of the IEEE,* Vol. 67, pp. 1092-1114

[48] Bertoni, H. L. (1985). Rayleigh Waves in Scanning Acoustic Microscopy. *Ash EA, Paige EGS, editors. Rayleigh-Wave Theory and Application. The Royal Institution, London,* Vol. 2, pp. 274-290

[49] Liang, K. K., Kino, G. S. and Khuri-Yakub, B. T. (1985). Material Characterization by the Inversion of V(Z). *IEEE Transactions on Sonics and Ultrasonics,* Vol. SU-32, No. 2, pp. 213-224

[50] Matikas, T. E., Rousseau, M. and Gatignol, P. (1992). Experimental Study of Focused Ultrasonic Beams Reflected at a Fluid-Solid Interface in the Neighborhood of the Rayleigh Angle. *IEEE Transactions on Ultrasonics Ferroelectrics and Frequency Control,* Vol. 39, No. 6, pp. 737-744

[51] Blatt, D., Karpur, P., Matikas, T. E., Blodgett, M. P. and Stubbs, D. A. (1993). Elevated Temperature Degradation and Damage Mechanisms of Titanium Based Metal Matrix Composites with SCS-6 Fibers. *Scipta Metallurgica et Materialia,* Vol. 29, pp. 851-856

[52] Waterbury, M. C., Karpur, P., Matikas, T. E., Krishnamurthy, S. and Miracle, D. B. (1994). In Situ Observation of the Single-Fiber Fragmentation Process in Metal-Matrix Composites by Ultrasonic Imaging. *Composites Science and Technology,* Vol. 52, No. 2, pp. 261-266

[53] Cantrell, J. H. and Yost, W. T. (1994). Acoustic Harmonic Generation from Fatigue-Induced Dislocation Dipoles. *Philosophical magazine A,* Vol. 69, No. 2, pp. 315-326

[54] Granato, A. and Lücke, K. (1956). Theory of Mechanical Damping Due to Dislocations. *Journal of Applied Physics,* Vol. 27, pp. 583

[55] Planat, M. (1985). Multiple Scale Analysis of the Nonlinear Surface Acoustic Wave Propagation in Anisotropic Crystals. *J. Appl. Phys.,* Vol. 57, pp. 4911–4915

[56] Herrmann, J., Kim, J. Y., Jacobs, L. J., Qu, J., Littles, J. W. and Savage, M. F. (2006). Assessment of Material Damage in a Nickel-Base Superalloy Using Nonlinear Rayleigh Surface Waves, *Journal of Applied Physics,* Vol. 99, No. 12, pp. 124913

[57] Kim, J.-Y., Jacobs, L. J., Qu, J. and Littles, J. W. (2006). Experimental Characterization of Fatigue Damage in a Nickel-Base Superalloy Using Nonlinear Ultrasonic Waves. *J Acoust Soc Am,* Vol. 120, No. 3, pp. 1266-1273

[58] Shui, G., Kim, J. Y., Qu, J., Wang, Y.-S. and Jacobs, L. J. (2008). A New Technique for Measuring the Acoustic Nonlinearity of Materials Using Rayleigh Waves. *NDT&E International,* Vol. 41, pp. 326-329

[59] Shull, D. J., Hamilton, M. F., Ilinsky, Y. A. and Zabolotskaya, E. A. (1993). Harmonic Generation in Plane and Cylindrical Nonlinear Rayleigh Waves. *J. Acoust. Soc. Am.,* Vol. 94, pp. 418-427

[60] Zabolotskaya, E. A. (1992). Nonlinear Propagation of Plane and Circular Rayleigh Waves in Isotropic Solids. *J. Acoust. Soc. Am.,* Vol. 91, No. 5, pp. 2569-2575